energies

MDPI

Article

Fractional Chaos Maps with Flower Pollination Algorithm for Partial Shading Mitigation of Photovoltaic Systems

Dalia Yousri [1], Thanikanti Sudhakar Babu [2], Dalia Allam [1], Vigna. K. Ramachandaramurthy [2], Eman Beshr [3,*] and Magdy. B. Eteiba [1]

1 Electrical Engineering Department, Faculty of Engineering, Fayoum University, Al Fayoum, Fayoum 63514, Egypt
2 Institute of Power Engineering, Department of Electrical Power Engineering, Universiti Tenaga National, Jalan IKRAM-UNITEN, Kajang 43000, Malaysia
3 Electrical and Control Engineering Department, Arab Academy for Science, Technology, and Maritime Transport, Sheraton Al Matar, P.O.2033 Elhorria, Cairo 11311, Egypt
* Correspondence: beshre@aast.edu; Tel.: +20-1114153334

Received: 7 August 2019; Accepted: 9 September 2019; Published: 16 September 2019

Abstract: Solar Photovoltaic (PV) systems have become prominent and have attained the attention of energy engineers, governments and researchers. To achieve the maximum benefit from the PV system in spite of its nonlinear characteristic and environmental conditions, finding a robust maximum power point tracking method is essential. Over two decades, various researchers proposed numerous MPPT methods, but they failed to evaluate their methods on consistency, reliability, and robustness over several numbers of runs. Most of the researchers examined one configuration and they did not to consider the dynamic change in the irradiation conditions. Therefore, in this manuscript, the authors introduced a novel optimization technique Fractional chaotic Flower Pollination Algorithm (FC-FPA), by merging fractional chaos maps with flower pollination algorithm (FPA). The proposed technique, help FPA in extracting the Global Maximum Power Point (GMPP) under different partial shading patterns including with different PV array configurations. The proposed FC-FPA technique is tested and evaluated over 5 different patterns of partial shading conditions. The first three patterns are tested over 4S configuration made with Shell S36 PV module. The other two patterns are applied to the 4S2P configuration of Shell SM55 PV panels. The performance of the proposed variant is investigated by tracking the GMPP for abruptly changing shade pattern. Exclusive statistical analysis is performed over several numbers of runs. Comparison with perturb and observe MPPT technique is established. These results confirm that, the proposed method shows fast convergence, zero oscillation and rapid response for the dynamic change in irradiation with consistent behavior.

Keywords: maximum power point tracker; partial shading conditions; flower pollination algorithm; fractional chaos maps

1. Introduction

The development of renewable energy resources have been drastically increases due to the effect of greenhouse gases, depletion of fossil fuels and high demand of electricity [1]. Solar photovoltaic (PV) generation has excellent potential due to the absence of fuel cost and limited maintenance compared to other energy resources [2]. Based on the World Energy Outlook 2018 reports, the PV power generation will become increases significantly by 2040 and exhibits a higher global generation capacity than all other forms of energy [3]. The PV generated power greatly depends on the environmental conditions like irradiation and temperature as well as the partial shading (PS) phenomena. These factors drastically

reduces the PV generated power [4,5]. Researchers focused to develop maximum power point tracking (MPPT) techniques [6] to reduce the influence of these factors and to improve the PV system efficiency. The non-linear characteristics of solar PV, and partial shading condition causes multiple peaks on the P-V characteristics. However, to reduce these multi-peaks into a global peak is a challenging task [7].

With this inspiration, researchers and practitioners developed numerous MPPT techniques which can be categorized into two types based on their implementation. Those are traditional MPPT techniques and soft computing techniques. The traditional MPPT methods like perturbation and observation (P&O) [8], hill climbing (HC) [9] and incremental conductance (IncCond) [10] are widely used due to simplicity in design, easy implementation, replicates less number of sensors. Despite of these features, P&O method suffers from a high rate of perturbations and generates more oscillations around maximum power point (MPP). The IncCond method exhibits weak convergence, and the HC method is suitable only for low power applications. Moreover, these three methods are failed to achieve global peak under rapid irradiation changes [1].

The evolutionary techniques were widely preferred and developed as they overcome the drawbacks of traditional methods like fixed step size. In addition, few other advantages like, capability of handling non-linear and multi-modal objective functions, extensive exploration in search space [11] increases the development of evolutionary techniques. Thereby, numerous optimization algorithms have been developed by various researchers. Notable algorithms proposed in the recent years are, moth-flame optimization algorithm (MFO) [12], ant colony optimizer [13], bat algorithm [14], flower pollination algorithm (FPA) [15,16], non-linear backstepping control technique [17], mine blast optimization (MBO) and teaching learning-based optimization (TLBO) algorithms [18,19], golden section search based algorithm [20], bypass diode scanning algorithm [21] and wind-driven optimization (WDO) algorithm [22]. The modified versions of stochastic algorithms are introduced such as modified cat swarm optimization (MCSO) [7], improved particle swarm optimization (IPSO) [23], modified PSO (MPSO) method is presented in [24], and a new version of PSO named leader PSO (LPSO) is proposed in [25]. Additionally, other MPPT methods are proposed to alleviate a random number in conventional cuckoo search (CS) algorithm [26] whereas Distributed MPPT technique is proposed in [27].

Another new trend named hybrid techniques were introduced to improve the performance of classical algorithms. In this, the properties of two or more meta-heuristic optimization algorithms are combined or hybridized between the conventional methods with the meta-heuristic optimization techniques. A simplified accelerated particle swarm optimization (SAPSO) was proposed in [28] by combining a variant of the particle swarm optimization (PSO) algorithm and the classical HC algorithm. Hybrid gaussian process regression-jaya (GPR-Jaya) algorithm in [29] improved the performance of jaya algorithm by introducing the GPR model. Other hybrid grey wolf optimization with fuzzy logic control (GWO-FLC) method is proposed to solve the problem of Local maximum power point (LMPP) and oscillations around Maximum power point (MPP). Another advanced searching technique named PSO-based MPPT algorithm TSPSOEM is proposed [30] by utilizing properties of particle swarm optimization (PSO) and shuffled frog leaping algorithm (SFLA). The other hybrid method proposed by incorporating properties of FLC and three-point weight method in [31].

Another novel method using artificial vision to track MPP is proposed by authors in [32]. In this method, a webcam is used to recognize the shadow irradiation progressively and give the reference voltage that supplies the maximum power irrespective of the number of peaks on the P-V curve. This method requires high efficient webcams, which increases the cost.

From the presented literature, it is understood that, there exist some limitations in the methods, that are listed as follows:

- Conventional MPPT techniques may settle at any one of LMPP. Adaptive step-size methods take a longer time to reach MPP. In addition, these methods require complex calculations to estimate step size and exhibits slow convergence. Further, these methods are more efficient, only in-case of uniform irradiation conditions [33].

- For the evolutionary algorithm (EA) based MPPT techniques, the commonly noticeable drawbacks are the trade-off between exploration-exploitation which is very less, which results in fluctuations during the process of optimization. These methods may fall in LMPP during wider (strong) shading conditions. In addition, these methods fail to reach new GMPP once they change their position since the search particles will be busy around previous MPP and lack of consistency [34]. Therefore, due to these limitations, the efficiency of the system will get reduce. Additionally, that open-up a room to improve the performance of MPPT techniques further.

The various research gaps observed from the literature review are summarized in Table 1.

Based on the previous limitations and gap analysis, it is noted that none of the researchers have made an attempt to involve the chaotic features into MPPT, which extensively increases the performance of non-linear objectives. The chaos theory to improve meta-heuristic optimization algorithms has become the dominant topic in the field of optimization algorithms. The dynamical and randomization properties of chaos maps help the optimization algorithms to balance between the intensification (exploitation) and diversification (exploration) phases [35,36].

With this motivation, authors introduced new MPPT technique titled novel fractional chaotic flower pollination algorithm (FC-FPA) with a combination of fractional order chaos maps.

The dynamic properties of fractional order chaos maps enhances the perofrmance of meta-heuristic algorithms. This has not been implemented by any of the researcher so far. Therefore, in this article, authors proposed a new and unique technique of introducing chaotic variants to achieve the GMPP irrespective of environmental conditions, type of PV module, uniform and dynamic change in irradiation conditions. In the proposed FC-FPA technique, three fractional chaos maps are co-operated with the FPA algorithm for the initialization phase and for tuning its parameters. The considered fractional chaos maps are fractional logistic map, fractional sine map, and fractional tent chaos map.

The main contributions of the paper are:

- In this article authors introduced a unique novel method of chaotic variants (based on fractional-order chaos maps) to track maximum power point.
- The proposed method is tested with two different types of models under two configurations like Multi-crystalline type (S36) with four series combination (4S) and Mono-crystalline type (SM55) PV model with four-series-two-parallel (4S2P) configuration.
- The effectiveness of the proposed method is validated using 3 different shade pattern with above mentioned configurations.
- The robustness of the algorithm variants are evaluated in tracking the GMPP during a sudden change in the irradiation conditions.
- The proposed variants are compared with the basic version of the FPA algorithm over all the stages of analysis.
- Extensive statistical analysis has been performed to demonstrate the superiority of the proposed variants and recommended the best chaos map that helps the FPA in achieving fast-tracking for GMPP with most consistent and accurate behavior.
- The recommended MPPT algorithm variant is compared with the traditional perturb and observe MPPT (P&O) over the nonuniform distribution of radiation and step change in its levels.

Table 1. Research gaps and noticeable remarks on recent published MPPT algorithms.

Authors	Year	Algorithms	Control Parameter	Remark	Gap of Analysis
[37]	2019	Improved FLC	Duty cycle	The converging speed for transients is improved and oscillations around the MPPs are completely eliminated compared with conventional MPPT methods, Single pattern is used solar PV module of MSX-60W, Proposed method is compared with these two algorithms P&O, FLC-HC.	No dynamic performance, no statistical metrics.
[29]	2019	hybrid GPR-JAYA	Voltage	The method is tested under different shade patterns of 3S, 5S and 4S3P designed with PV model of CS6P-260 P. It is compared with standard PSO and Jaya algorithms. Mean, and standard deviation (SD) was considered evaluating system performance.	Controlled voltage source is used instead of the converter, how far it will be reliable in real-time conditions. The authors proposed only two patterns of shading moreover their algorithm was not tested with the dynamical changes of irradiance.
[38]	2019	Drift free technique adopted to inc	Duty cycle and voltage	Using drift free technique with the help of only one voltage sensor the mppt has been proposed for inc method. Thereby implementation cost is reduced. The maximum efficiency of 97.65% is achieved.	Implemented over a single panel by changing irradiation for a certain period of time. No dynamic performance, not tested under PSC with multiple panels, No metrics, solar PV emulator is used instead of real PV module.
[34]	2019	Hybrid GWO-FLC	Duty cycle	Hybrid GWO-FLC is implemented to overcome the drawbacks of reaching GMPP using GWO, and reducing oscillations with help of FLC. The proposed method is compared with PSO, GWO.	In this article duty cycle initialization is done based on predefined time of 24 s, this is not accurate since the shade may occur at any point of time, in addition, initialization is fixed based on the occurrence of partial shade irrespective of voltage or current variations.
[22]	2019	WDO	Duty cycle	WDO is introduced to improve the efficiency and tracking speed of MPPT. Kyocera KD135SX-UPU PV model used, the proposed method is compared with various existing methods, namely WDO, PSO, DE, HSA, Bat, SCA, CS, and GA. In addition, presented seven statistical metrics to show the accuracy of the method.	The authors did not test the introduced algorithms for dynamic change in radiation while they only tested their algorithms for the static ones. All the algorithms employed for only one module and one configuration.
[39]	2018	Improved DE	Duty cycle	Improved DE algorithm was proposed. The tracking time and efficiency are 2 s and 99%, respectively. The test is performed on a string of 10S PV-UE125MF5N PV model. SEPIC converter is used.	The authors did not test the introduced algorithms for dynamic change in radiation only test their algorithms for the static ones. No statistical analysis is included in the manuscript the algorithm tested for only one run.
[40]	2018	GA	Duty cycle	Proposed GA algorithm to improve the convergence, rapidity, and accuracy of the PV system. It is compared with conventional P&O and INC method.	Tested with a single PV module with different shade pattern, while the authors did not consider partial shade and dynamic shade.
[14]	2018	Bat	Duty cycle	Bat algorithm is proposed in comparison with PSO, DE, and P&O methods. Three shade conditions with the 4S structure are presented. SEPIC converter is used.	The authors did not test the introduced algorithms for dynamic change in radiation, only test their algorithms for the static ones. Only one module and one configuration are utilized in the validation of the performance of the algorithms. No statistical analysis are performed.

Table 1. *Cont.*

Authors	Year	Algorithms	Control Parameter	Remark	Gap of Analysis
[15]	2017	FPA	Duty cycle	Proposed basic FPA and compared with P&O and PSO. Tested with three shade patterns of 4S configurations designed with Shell S36 PV module. The efficiency is 99.85% and taking 0.45 s to achieve mpp .	Authors failed to present statistical analysis. The system is less consistent. The robustness of their algorithm was not tested where the authors introduce only one run for their algorithm. Shell S36 PV module was the only PV module type used in the simulation part.
[25]	2017	LPSO	Duty cycle	Proposed LPSO and tested with three different shade patterns of 6S configuration made-up of with Kotak 80W panel. Results compared with basic P&O and PSO.	Authors did not perform any statistical analysis to show the consistency and robustness of their method. Only one module employed in the manuscript.
[28]	2018	SAPSO	Duty cycle	SAPSO is a variant of PSO and HC; it is tested with the configuration of two panels in series.	SAPSO was not be tested under dynamic variations, and partials shaded conditions. Attained convergence on 3.4 s for 2S configuration.
[7]	2018	MCSO	Duty cycle	MCSO is proposed to achieve GMPP, and tested system three shade patterns of configuration 5S made with MSX-60 PV module.	MCSO is compared with other methods like PSO, MPSO by performing a single run, which will show less consistency. Convergence speed and any sort of statistical analysis are not performed.
[12]	2018	MFO	Duty cycle	MFO is proposed as a solution to PSC, and it is compared with IncCond, FL-IncCond, PSO. Sun Power SPR- 305 WHT-U PV module is used.	The MFO is tested under two different ratings as 100 kW array and for 1MW power plant. Achieved efficiency of 99.91% Authors did not discuss convergence speed; efficiency is calculated with a single run, didn't perform any statistical analysis.
[30]	2018	TSPSOEM	Duty cycle	A new hybrid TSPSOEM algorithm with the combination of PSO and SFLA is proposed for the DMPPT. Implemented for a grid connected system, it is compared with conventional P&O and PSO.	Attained an efficiency of 95.7%, the method is not tested under dynamic conditions and they did not perform any sort of statistical analysis to show the robustness of method.

The organization of the manuscript is as follows; Section 2 discusses the photovoltaic modeling, DC-DC boost converter, and the effect of the PSC over the considered PV system. Section 3 contains the proposed optimization algorithm variants, and implementation steps for the application of MPPT. Section 4 discusses the results and analysis. Section 5 exhibits the comparison between the recommended MPPT variant and P&O technique. Finally, Section 6 summarizes the main outcomes and the conclusions.

2. System Description

The schematic diagram of the considered system in the current investigation is shown in Figure 1. The considered PV configuration is connected to the DC-DC boost converter connected to resistive load. The described models for the elements in the system are presented as follows;

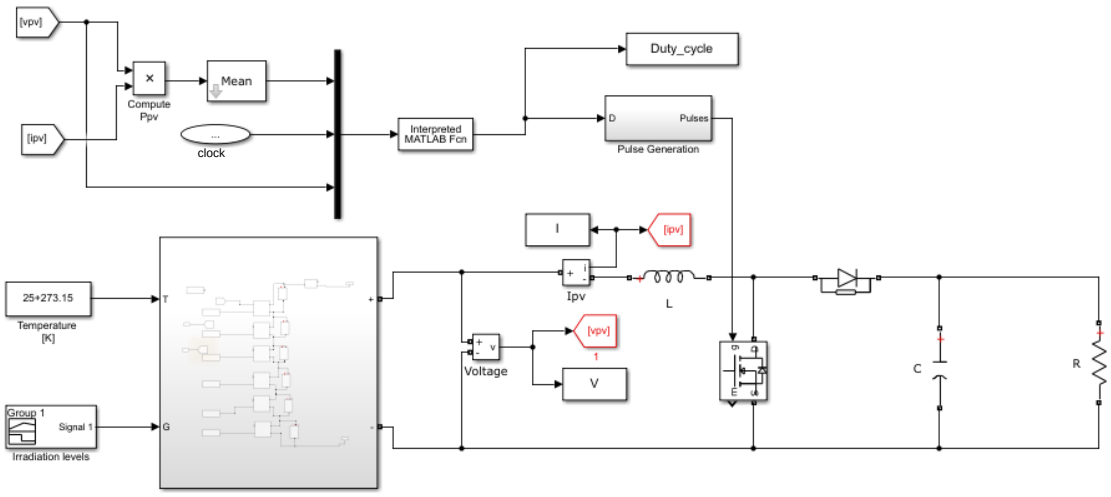

Figure 1. Matlab simulink scheme with boost converter.

2.1. Photovoltaic Models

The PV module is an important element of any PV plant. The accurate modeling of solar PV cell is imperative due to the drawbacks, namely 1. current-voltage (I-V) and power-voltage (P-V) characteristics of PV are profoundly non-linear. 2. These two characteristics are highly affected by environmental conditions [7]. Numerous work have been carried-out by researchers to design an accurate solar PV cell using number of diodes. The widely available models in the literature are single diode model (SDM) [41], double diode model (DDM) [42] and triple diode model (TDM) [43]. The SDM is considered as a dominant one in diverse fields of applications due to its vibrant advantages namely simple in design, good in accuracy and less number of parameters involved (five parameters only) [24]. Therefore, in this paper, SDM is utilized to emulate the behavior of two different PV modules (Shell S36 and Shell SM55) under various environmental conditions as presented by the authors in [41]. The equivalent circuit of SDM is shown in Figure 2. It is comprises with current source (I_{pv}) and a diode D is connected anti-parallel to it. Series resistance (R_s) and shunt resistance (R_p) indicates contact and leakage losses respectively [24]. The total current generated by PV module can be estimated by applying KCL to circuit and final current equation can be written as in Equation (1).

$$I = I_{pv} - I_o \left[exp\left(\frac{(V + IR_s)}{a} \right) - 1 \right] - \frac{(V + IR_s)}{R_p} \quad (1)$$

where, I_{pv}, I_o, R_S and R_P are respectively PV current, leakage current, series and shunt resistance. a is modified ideality factor of a diode D. a can be defined as given in Equation (2)

$$a = \frac{N_{ss} n_I k T}{q} \tag{2}$$

where, k is Boltzmann constant and its value is $1.35 \times 10^{-23} J/K$, T represents temperature of a PV cell in Kelvin, q and N_{ss} are charge of electron (1.6×10^{-19} C) and number of cells in series. n_I represents usual ideality factor. I_{PV} and I_o can be calculated by using the Equations (3) and (4) as presented by authors in [44].

$$I_{pv} = [I_{pv_{STC}} + k_i(T - T_{STC})] \frac{G}{G_{STC}} \tag{3}$$

$$I_o = \frac{I_{SC-STC} + k_i(T - T_{STC})}{exp\left(\frac{q(Voc-STC)+k_v(T-T_{STC})}{n_I k T}\right) - 1} \tag{4}$$

where, k_i is coefficient of short circuit current, $I_{pv_{STC}}$ represents pv current under standard test conditions (STC), it defines the temperature and irradiation are 25 °C and 1000 W/m^2 respectively. k_v is coefficient of open circuit voltage, I_{SC-STC} and V_{OC-STC} are the short circuit current and open circuit voltage under STC, respectively.

Further to calculate the total current generated by PV module under partial shading condition, the Equation (1) can be modified and is presented as in Equation (5) [25].

$$I = I_{pv} N_{pp} - I_o N_{pp} \left[exp\left(\frac{(V + IR_s(N_{ss}/N_{pp}))}{a}\right) - 1 \right] - \frac{(V + IR_s(N_{ss}/N_{pp}))}{R_{pv}(N_{ss}/N_{pp})} \tag{5}$$

where, N_{pp}, N_{ss} represents number of parallel and series connected PV modules.

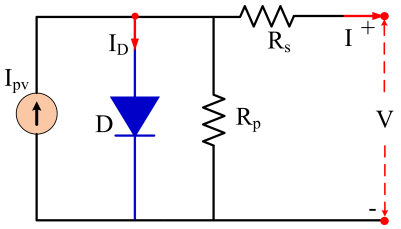

Figure 2. Equivalent circuit of single diode PV model.

2.2. Boost Dc-DC Converter

To implement the proposed MPPT technique, Boost converter is considered as a interfacing device between the input and load. To design the suitable rated boost converter the relationships between input and output voltages are given as follows:

$$V_{out} = \frac{V_{in}}{1 - D} \tag{6}$$

$$I_{out} = (1 - D) I_{in} \tag{7}$$

The equivalent resistance of a boost converter can be estimated using the formula given in Equation (8):

$$R_{eqiv} = (1 - D)^2 R_{load} \tag{8}$$

where, V_{out}, V_{in} represents output and input voltage of boost converter, D indicates the operated duty cycle, R_{load} is treated as load resistance of boost converter, and R_{equiv} is equivalent resistance of sytem which helps to achieve the maximum power. Based on the simulation diagram of the studied system in Figure 1, the boost converter with input inductance of 30 mH, output capacitor value 100 µF, connected to resistive load of 100 Ω and operating at switching frequency 10 kHz is considered. The experimentation's were performed using MATLAB simulink.

2.3. Partial Shading and Its Effects

In practical scenario, a single PV module cannot produce the required amount of power. Thereby, a number of PV modules are connected in combinations of series and parallel [45]. The maximum power yield by PV modules is mainly depending on environmental conditions like irradiation and temperature. Due to these environmental changes, all the PV modules may not receive equal amount of irradiation. This phenomenon is known as partial shading. In addition, the partial shading is also caused by reasons like passing of clouds, tree and building shadow and birds droppings [46,47]. This partial shading phenomena results in hot-spots over the PV panels. During shade conditions, the shaded panel acts as a load instead of source. With this, the particular PV panel undergoes high current stress and temperature which causes the damage of shaded panel. To overcome this hot-spots, a bypass diode D_b is connected parallel to each PV module, as it behaves as a high resistance ($R_b = 10^{10}\,\Omega$) in the reverse-biased mode and low resistance ($R_b = 10^{-2}\,\Omega$) in the forward-biased based on the following relation [48].

$$I > I_{pv}, \tag{9a}$$

$$R_b(I) = \begin{cases} 10^{-2} & D_b \quad on \\ 10^{10} & D_b \quad off \end{cases} \tag{9b}$$

Moreover, blocking diode is connected to avoid the reverse flow of current as shown in Figures 3a and 4a, respectively.

To illustrate the effect of partial shading, two configurations of different PV modules are considered as presented below:

- The first configuration is designed as 4 PV modules connected in series to form a string. This string is made of Shell S36 Multi-crystalline PV module. Under this configuration, 3 different shading patterns are considered and that are presented Figure 3a.

  The specifications of this module are presented in Table 2.

  - Pattern 1 (no shade condition), In this, 4 PV modules receives equal (uniform) irradiation levels i.e., 1000 W/m^2
  - Pattern 2 (partial shade condition), in this pattern, modules M_1, M_2 receives 1000 W/m^2 and M_3, M_4 are subjected to receive 300 W/m^2
  - Pattern 3 (heavy shade condition) M_1, M_2, M_3 and M_4 receives irradiation's of 1000 W/m^2, 700 W/m^2, 500 W/m^2, 300 W/m^2 respectively. This shade pattern is considered for effective analysis of system under heavy shade conditions.

- The second configuration is made with a structure of 4 series panels with 2 parallel strings (4S2P). This configuration is made up of with Shell SM55 of Mono-crystalline type. This configuration is specifically designed to test the proposed method even for high rated PV systems. Under this configuration, two different shading patterns are tested as shown in Figure 4a

  - Pattern 4, the PV modules M_{11}, M_{12}, M_{21}, M_{22} receives 1000 W/m^2, M_{31}, M_{32} are subjected to receive 500 W/m^2 and M_{41}, M_{42} receives 300 W/m^2.
  - Pattern 5, the PV modules M_{11}, M_{12} receives 1000 W/m^2, M_{21}, M_{22} receives 900 W/m^2, M_{31}, M_{32} receives 600 W/m^2 and M_{41}, M_{42} receives 300 W/m^2.

The specifications of $S36$ and $SM55$ module are presented in Table 2. The two configurations were tested under a constant temperature of 25 °C, and a detailed analysis under these configurations are presented in the below section.

In the case of pattern 1, the 4 PV modules will generate an equal amount of current due to the presence of uniform irradiation of 1000 W/m^2 across all the panels. During this scenario, bypass diode

acts as reverse bias. Therefore, it generates a complete I-V curve without any steps on it, as shown in Figure 3b of pattern 1. Further, the total power produced by the string is equal to the sum of individual panel powers. It provides a single peak $(P1)$ on P-V curve as shown in Figure 3c.

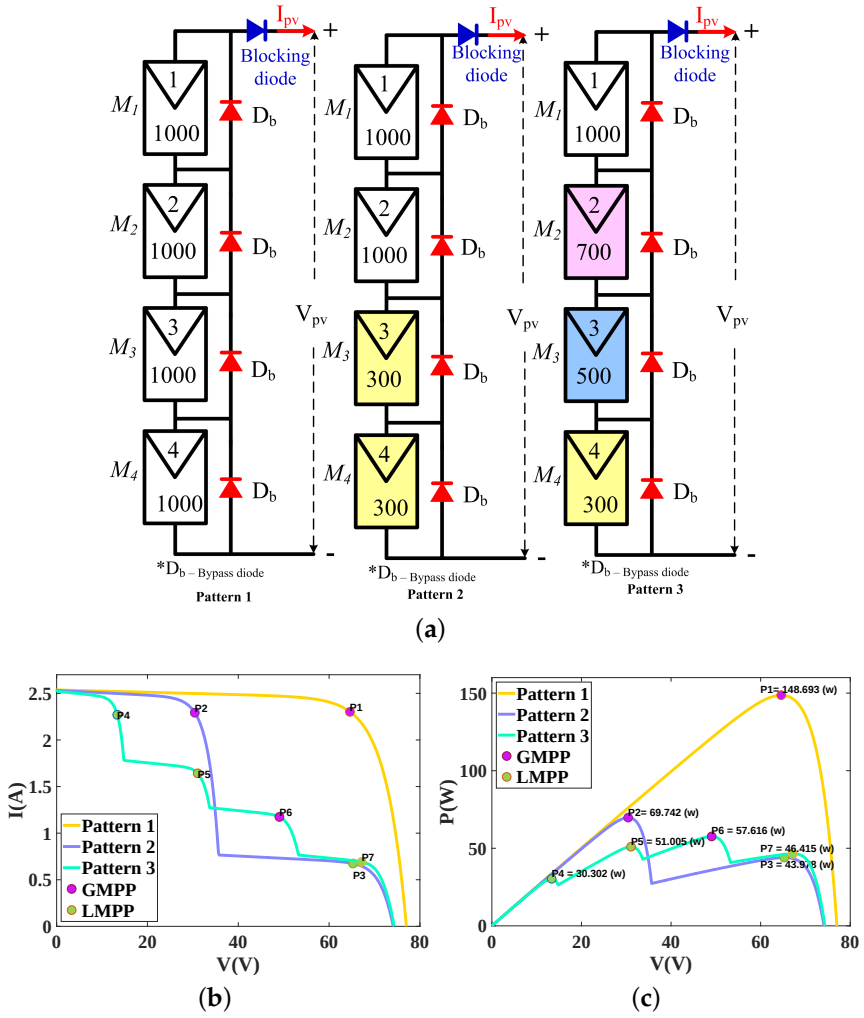

Figure 3. Partial shading analysis on S36 PV module (**a**) Shading patterns patterns, (**b**) I-V curves and (**c**) P-V curves.

Table 2. Specifications of solar PV modules.

Parameters	PV Modules	
	S36	SM55
Type of cell	Multi-crystalline	Mono-crystalline
Rated power	36 W	55 W
Peak power voltage (V_{mpp})	16.5 V	17.4 V
Peak power current (I_{mpp})	2.18 A	3.15 A
Open circuit voltage (V_{oc})	21.4 V	21.7 V
Short circuit current (I_{sc})	2.30 A	3.45 A
Current temperature coefficient (k_i)	0.001 A/K	+1.4 mA/°C
Voltage temperature coefficient (k_v)	−0.76 V/K	−76 mV/°C
No. of series cells	36	36
Cell dimensions	125.0 × 62.5 mm	103 × 103 mm

During partially shaded conditions, the PV modules will receive different irradiation's. For more understanding of this effect, pattern 2 is considered with two different irradiation levels. Due to this

shade difference, the PV modules M_1, M_2 and M_3, M_4 generate different currents, thereby steps in I-V characteristics of pattern 2 can be observed in Figure 3b. This results two peaks $(P2, P3)$ on P-V curve as shown in Figure 3c of Pattern 2. Similarly based on the irradiation presence on Pattern 3, it will generate four different currents thereby it results four steps and four peaks ($P4$, $P5$, $P6$, $P7$) on I-V and P-V curves respectively as shown in Figure 4b,c of pattern 3. For understanding these multiple peaks on P-V curves, the simulations have been carried out as per the shade patterns are shown in Figure 3a. The resultant P-V and I-V curves are plotted with different colors to differentiate the power differences among shading patterns along with its captured powers. Among these peaks over P-V curves, $P1$, $P2$, and $P6$ are considered as global maximum power points (GMPP) for the shade patterns 1, 2 and 3 respectively. The remain other points ($P3$, $P4$, $P5$ and $P7$) are treated as local maximum power points (LMPP).

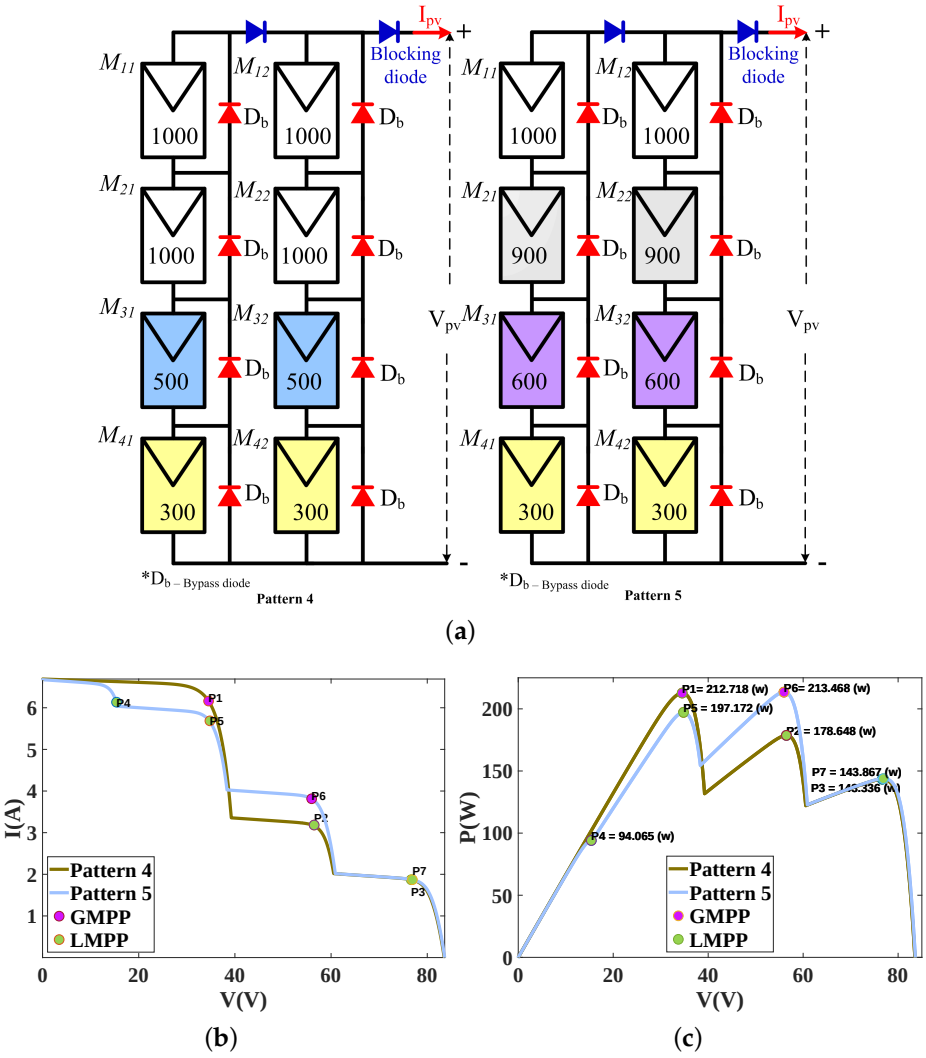

Figure 4. Partial shading analysis on SM55 PV module (**a**) Shading patterns patterns, (**b**) I-V curves and (**c**) P-V curves.

Additionally, for more critical analysis and to verify the proposed method even under high power rated systems, the second configuration 4S2P of shell SM55 make is considered. The considered patterns under this configuration are shown in Figure 4a. The similar procedure has been carried out for the second configuration of pattern 4 and 5 as implemented for configuration 1. Based on the shades present on pattern 4 and 5, after performing the simulations, the multiple peaks and steps

on P-V and I-V curves exist as shown in Figure 4b,c. The respective power values are presented in Figure 4c to indicate the difference in power generation among shading patterns 4 and 5. Further the peak points $P1$ and $P6$ refers to GMPP of patterns 4 and 5 respectively, and all other peak points $P2$, $P3$, $P4$, $P5$ and $P7$ represents LMPP.

To track the GMPP with the presence of multiple peaks in the P-V characteristics, introducing a robust maximum power point tracking algorithm is still required. Therefore, in the next sections, novel variants flower pollination algorithm is introduced and investigated over the 5 shade patterns. Moreover, the performance of the proposed variants are evaluated under dynamic change in irradiation. The dynamic change in irradiation is considered as by changing modules irradiation from, pattern 1 to pattern 2 and then to pattern 3. Similarly from pattern 4 to pattern 5.

3. Proposed Novel Chaotic Flower Pollination Algorithm

In this section, the description of the proposed algorithm is explained in detail. The implementation steps towards the application of MPPT are presented.

3.1. Fractional Chaotic Flower Pollination Algorithm Variants (FC-FPA)

FPA technique was introduced by Yang in [49] to emulate the natural phenomena of pollination in plants. FPA and other meta-heuristic optimization algorithms depends on the Gaussian or uniform distributions to fulfill its randomization, during the initialization or implementation stage. Recently, researchers have introduced another method to improve the performance of the basic version of the algorithms by replacing these distributions. Chaos theory is an alternative approach for these distributions and become a new trend in the modification of the optimization algorithms [36,50]. Chaos is a deterministic, pseudo-random, non-converging, non-period and bounded method can be found in non-linear dynamical systems [51]. Several attempts were made to prove that the randomness and the dynamical properties of the chaos maps help the optimization techniques to overcome from local optima [52–54]. Therefore, in this paper, by recognizing the importance of chaotic maps in improving the accuracy, consistency and convergence speed of the basic algorithms, the authors are motivated to employ a new version of these maps named fractional chaotic maps as the first time in MPPT application. As the fractional chaos maps have another new dynamical distribution, the authors tested them in MPPT to endorse a suitable map provides an efficient performance over this application.

The implemented maps are the fractional logistic, sine and tent maps in addition to their standard version. The mathematical formulas for the handled maps are presented below.

The considered Fractional logistic map can represented mathematically as:

$$x_{T+1} = x_0 + \frac{\mu}{\Gamma(\alpha)} \sum_{j=1}^{T} \frac{\Gamma(T-j+\alpha)}{\Gamma(T-j+1)} x_{j-1}(1-x_{j-1}), \quad \mu = 2.5, \alpha = 0.3 \tag{10}$$

The equation of Fractional sine map can given as:

$$x_{T+1} = x_0 + \frac{\mu}{\Gamma(\alpha)} \sum_{j=1}^{T} \frac{\Gamma(T-j+\alpha)}{\Gamma(T-j+1)} sin(x_{j-1}), \quad \mu = 3.8, \alpha = 0.8 \tag{11}$$

The mathematical representation of Fractional Tent map can be give as:

$$x_{T+1} = x_0 + \frac{1}{\Gamma(\alpha)} \sum_{j=1}^{T} \frac{\Gamma(T-j+\alpha)}{\Gamma(T-j+1)} min\left((\mu-1)x_{j-1}, \mu-(\mu+1)x_{j-1}\right), \quad \mu = 1.9, \alpha = 0.6, \tag{12}$$

where, T is the number of iterations. x_0 indicates the initial value is 0.7 [36].

The listed maps are employed in two phases; in the initialization stage and in modifying the random variables in the main control equations of FPA. The main differences between FPA and FC-FPA variants can be summarized as follows in Table 3.

Table 3. Main difference between FPA and FC-FPA based on MPPT.

		Algorithms		
Features		**FPA**	**FC-FPA**	**Remark**
1	Initialization	$Z_i = rand. * (Ub_i - Lb_i) + Lb_i$	$Z_i = C_j(i). * (Ub_i - Lb_i) + Lb_i$	The initial solution vector in FPA is computed randomly, but in case of FC-FPA, the initial vectors were calculated chaotically based in selected map $C_j(i)$
2	Switching probability factor between local and global search P	0.8	$C - P_j(T) = \frac{\left(C_j(T) - min(C_j)\right) * (P_{Max} - P_{Min})}{\left(max(C_j) - min(C_j)\right)} + S_{Min}$,	P in FPA are selected randomly based on uniform distribution. While in FC-FPA, it is adjusted by the suggested fractional chaos maps as in. Thereby $C-P$ is changed chaotically from 0.2 to 0.8 where the fractional chaos maps are normalized to be in the same interval $[0.2, 0.8]$.
3	Parameter ϵ	rand	$C\epsilon = C_j(T)$	ϵ is drawn from umiform distribution in the case of FPA whereas in FC-FPA, $C\epsilon$ is drawn from the chaotic maps with range $\in [0, 1]$

where, Z_i is the initial solution vector of the pollen i at iteration $T = 1$. $C_j(i)$ is the selected map with an index j, $min(C_j)$ and $max(C_j)$ are the minimum and maximum of the chaotic maps distribution. Ub and Lb are the upper and lower boundaries of the unknown variables. P_{Max}, P_{Min} are the required maximum and minimum values of P_j that are selected as 0.8 and 0.2, respectively.

3.2. Implementing FC-FPA as MPPT

The implementation steps of FC-FPA variants as MPPT technique are presented below and the same is represented in the form of flowchart as shown in Figure 5.

Step 1: Initialization: Define the initial parameters such as population size ($n = 5$), and maximum number of iterations $T_{max} = 27$. The upper and lower boundaries of the duty cycle ($Ub = 0.8$, $Lb = 0.2$). Select the index (j) of the chaos map (C_j) as $j = (1,2,3)$. Generate the initial values of the duty cycle ($d_i = Z_i$, $i = (1,2,3,\ldots,n = 5)$ chaotically for FC-FPA variants.

Step 2: Fitness evaluation: The panel voltage and current corresponding to the duty cycles $d_i, i = 1,2,3,\ldots,5$ $(d_1, d_2, d_3, d_4, d_5)$ are sensed and computes the corresponding fitness function $P_{pv_i} = P_{pv_1}, P_{pv_2} P_{pv_3} P_{pv_4} P_{pv_5}$. During the first iteration, store the global best value of the duty cycle (d_{Gbest}) that extracts the global maximum power $(G_{bes}) = (max(P_{pv_i}))$. In forth coming iterations d_{Gbest} and (G_{best}) are updated if the current power (P_{best}) is greater than the previous (G_{best}) power.

Step 3: Updating the duty cycle:
The $C - P$ and $C\epsilon$ values are determined in each iteration based on the chosen chaos map with index j. Then sending the updated duty cycle to the boost converter.

Step 4: Termination criteria: Aiming to achieve the fair comparison between the proposed variants and evaluating their stability towards converging to global solution during simulation, the termination criteria is verified in two different scenarios such as power deviation (ΔP_{pv_i}) [14] between the present and previous iteration is detected, the second one is that no deviation. Then the algorithm keep on converging for the GMPP until maximum number of iterations (maximum number of iterations 27) or completing the time of simulation which is selected as 4 s.

Step 5: Re-initialization process: The characteristics of the PV panels mainly depends on the environmental conditions thus with changing the shading pattern the MPP will be changed, if suddenly a large deviation (ΔP_{pv_i}) [14] between the power is detected. Hence the proposed MPPT technique should restart its search process to capture new GMPP and continues with steps 2 to 4 until get converge.

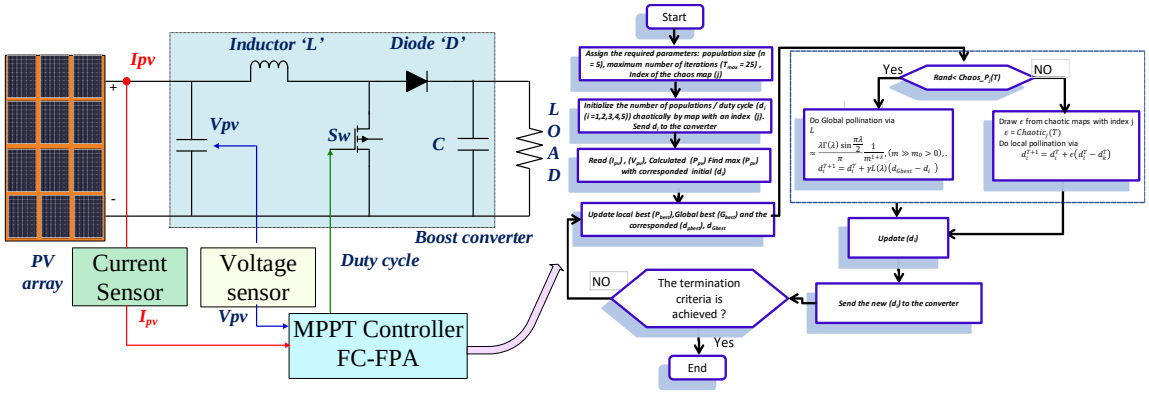

Figure 5. MPPT system design with the flowchart of FC-FPA.

4. Simulation and Results

To highlight the superiority of the proposed chaotic variants, the simulation results are compared with FPA. The simulations are carried-out for uniform and partial shade conditions using 4S and 4S2P configurations. A set of 5 shade patterns were tested and analyzed its performance. Several performance parameters like tracking speed, convergence time and efficiency are considered for evaluation. In addition, statistical analysis is performed to test the superiority and reliability of

the introduced variants. Each algorithm is simulated for 10 independent runs to perform statistical analysis. The formulae used for performing the statistical analysis are presented below:

$$Efficiency \quad (\eta) = \frac{P_{pv_{ei}}}{P_{pv_m}} * 100\% \tag{13}$$

$$Root\ Mean\ Square\ Error \quad (RMSE) = \sqrt{\frac{\sum_{i=1}^{K} \left(P_{pv_{ei}} - P_{pv_m}\right)^2}{K}} \tag{14}$$

$$Mean\ Absolute\ Error \quad (MAE) = \frac{\sum_{1}^{K} |P_{pv_{ei}} - P_{pv_m}|}{K} \tag{15}$$

$$Standard\ deviation \quad (STD) = \sqrt{\frac{\sum_{i=1}^{K} \left(P_{pv_{ei}} - \hat{P_{pv_{ei}}}\right)^2}{K}} \tag{16}$$

where, $P_{pv_{ei}}$, $\hat{P_{pv_{ei}}}$ and P_{pv_m} are the estimated for each run (i), the average power over number of runs and measured global PV power. K is the total number of the runs.

The schematic diagram of the setup shown in Figure 5. The considered PV configurations are connected to the DC-DC boost converter with input inductance of 30 mH, output capacitor value 100 µF, connected to resistive load of 100 Ω and operating at switching frequency 10 kHz. The experimentation's were performed using a laptop of Core i7-6500U CPU with 2.5 GHz of speed and 4 GB of RAM and "MATLAB 2018" environment.

The experimentation's carried-out under uniform and partial shading conditions are presented in the Section 4.1. In this subsection authors presented results obtained for both 4S and 4S2P configurations. To verify the performance of the system even under dynamic change in irradiation using different patterns are performed and are discussed in the Section 4.2.

4.1. Simulation Validation of Proposed Chaotic Variants in Comparison with FPA under Partial Shading Conditions

The performance of proposed system is analyzed under various parameters, the Section 4.1.1 deals the analysis based on tacking speed, computational time and accuracy. While the Section 4.1.2 is investigated based on the performed statistical analysis.

4.1.1. Tracking Speed, Time and Accuracy Factors

After performing the rigorous simulations over 4S configuration, the obtained mean convergence curves for the PV power, voltage, current and duty cycle are presented in Table 4. These plotted curves were obtained by performing number of independent runs.

1. **For the 1st string of 4S connected S36 modules**: three shade patterns are considered with the 1st configuration. The patterns 1, 2, and 3 indicate uniform, medium and heavy shade conditions respectively.

    - Pattern 1: a single global peak (GMPP) exists in the characteristics of the PV string at 148.693 W, it can be notice from Figure 3c of pattern 1. After performing the simulations with introduced variants the obtained convergence curves for Pattern 1 are presented in 1st row of Table 4. From the listed figures, it can be observe that, FPA tracks power of 145.336 W in 3.999 s including high oscillations around MPP and also there exist wide range of switching particles. FC-FPA variants (fractional logistic, fractional sine and fractional tent maps) able to track 148.513 W, 148.255 W and 148.514 W in a duration of 2.432 s, 1.228 s and 0.992 s respectively. From the figures it can be visualized that, the FC-FPA variants exhibits less number of oscillations around MPP and converges to maximum power than FPA in a less time period. The difference in power levels represents the poor exploitation capability of

FPA. FPA-fractional tent map shows better performance, it converges in 0.992 s which is saving 70% of tracking time and shows more stability than FPA.

- Pattern 2: Based on the receiving irradiation, pattern 2, generates two peaks over PV characteristics, as shown in Figure 3c. The two peaks occurred at power value of 69.742 W (GMPP), 43.978 W (LMPP) and are highlighting with points P2 and P3 respectively. After performing the simulations,the obtained convergence curves for Pattern 2 are presented in 2nd row of Table 4. FPA offers power value equaled to 69.623 W at 2.333 s with high amount of oscillations. FC-FPA variants (fractional logistic, fractional sine and fractional tent maps) tracks 69.71 W, 69.643 W, and 69.71 W in 1.433 s, 1.688 s and 1.353 s respectively. In this condition, it can be observe that, there exist negligible power difference between FPA and FC-FPA variants, however the FC-FPA variants converges in less time and than FPA. Fractional tent map converges in a very less time 1.353 s with minimal oscillations around MPP.
- Pattern 3 is considered as the strong shade condition as it receives nonhomogeneous irradiation levels. Sequentially four peaks are produced in the P-V characteristic, as shown in Figure 3. The GMPP located at 57.616 W and other LMPPs are located at 51.005 W, 46.415 W and 30.301 W, respectively. In spite of the rigorous test of pattern 3, the obtained plots are presented in last row of Table 4. From the plotted curves, it is observed that FC-FPA variants prove their robustness as they produce higher values of power in shorter tracking time. FPA tracks mean power 56.121 W at 3.33 s with high oscillation around MPP. The FC-FPA variants with fractional maps track 57.389 W, 57.424 W, and 57.467 W in 1.330 s, 1.681 s and 1.083 s, respectively. Therefore cooperating the fractional chaos maps with the basic version of FPA enhances in providing more power even under high shade conditions with reduced tracking time nearly for 50% from consumed by standard FPA and with zero fluctuation around MPP.

2. **For the 2nd configuration of 4S2P connected SM55 module**: Similar to the previous case, the mean convergence curves for the PV power, voltage, current and duty cycle for the Pattern 4 and pattern 5 are presented in Table 5. Pattern 4 and pattern 5 are derived for the configuration of 4S2P to test proposed method under high rated power capacity.

- Pattern 4: Due to the presence of different shades over Pattern 4, there exist three peaks and are shown in Figure 4c. Three power peaks are produced with magnitude of 212.718 W, 178.648 W, and 143.336 W. The GMPP is located at left side of PV curve with power values of 212.718 W. The obtained convergence curves for Pattern 4 are presented in 1st row of Table 5. From the presented figures it can be noticed that, FC-FPA variants shown their success in tracking the power which is closer to the GMPP in shorter period of time and achieves high stability compared with FPA. FC-FPA with fractional logistic map settles at values of 212.350 W, in 0.820 s. In the case of fractional sine map, the tracked power is 212.265 W at 1.358 s. The extracted power in case of fractional tent map is 212.452 W at 1.202 s. Meanwhile, FPA generates 205.254 W at 2.718 s with the presence of oscillations around MPP. Based on the obtained results, by using FC-FPA variants, able to track 3.4% power higher and also reduces 50% of tracking time than FPA. The attained 3.4% higher power reflects great significant in achieving more power in high rated PV systems which generates more income in less period of time.
- Pattern 5: The pattern 5 generates, four peaks in P-V curve can observe the same from Figure 4c. The power values of four peaks are 94.065 W, 197.172 W, 213.468 W and 143.867 W. The third peak *P*6 is the GMPP while the others are considered as LMPP. The last row of Table 5 shows the convergence curves plotted for the successful execution of pattern 5 using FPA and proposed FC-FPA variants. The three FC-FPA variants enhance their superiority as they track 213.156 W, 213.134 W and 213.089 W in 1.111 s, 1.562 s and 1.084 s, respectively. However, FPA generates power of 203.492 W in 1.931 s. The power generated by FPA is very

less than FC-FPA variants and consumes more time. There exit high amount of oscillations due to wide range of switching particles.

Table 4. Simulated mean power, and duty cycle of FPA and FC-FPA variants over number of runs for patterns 1, 2, and 3 of the 4S connected S36 PV array.

Simulation Analysis for 4S Connected S36 PV Modules	
PSC.	
Pattern 1	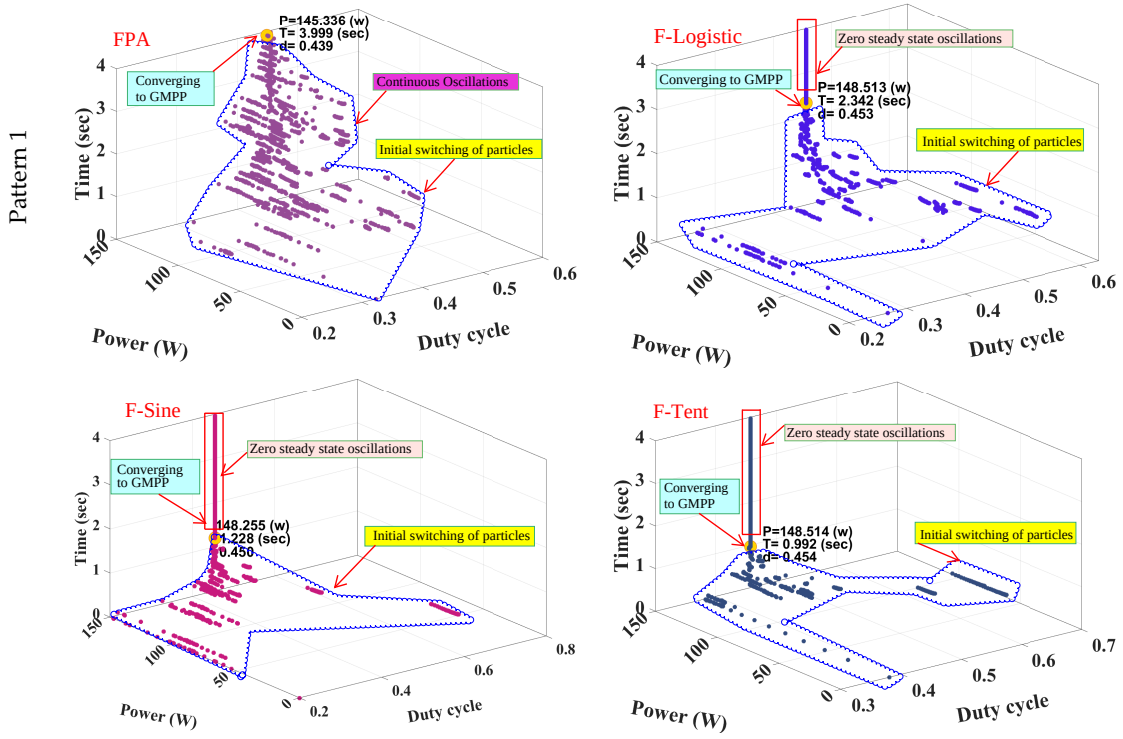
Pattern 2	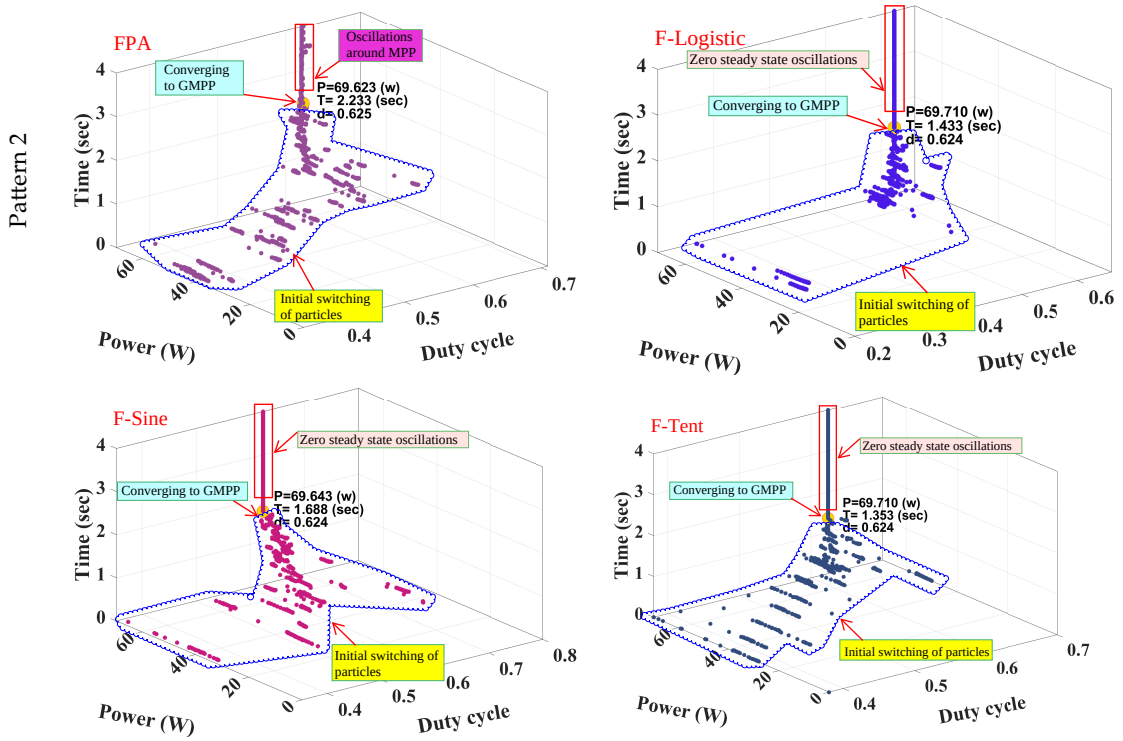

Table 4. *Cont.*

Simulation Analysis for 4S Connected S36 PV Modules	
PSC.	
Pattern 3	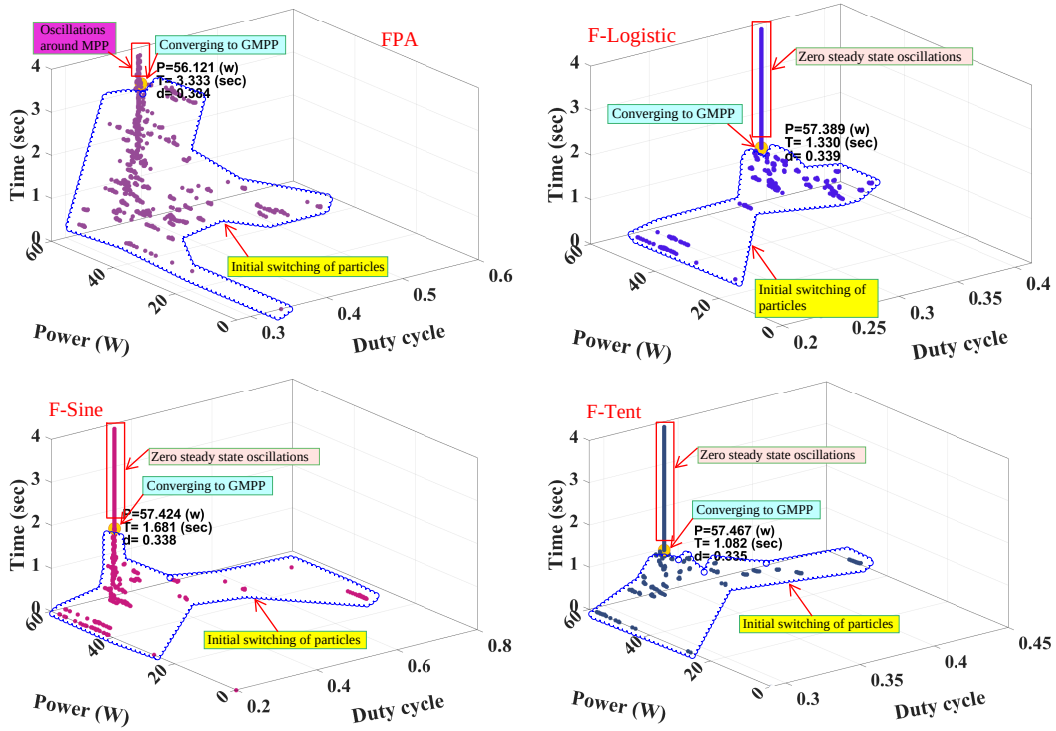

Table 5. Simulated mean power, and duty cycle of FPA and FC-FPA variants over number of runs for patterns 4, and 5 of the 4S2P connected SM55 PV array.

Simulation Analysis for 4S2P Connected SM55 PV Modules	
PSC.	
Pattern 4	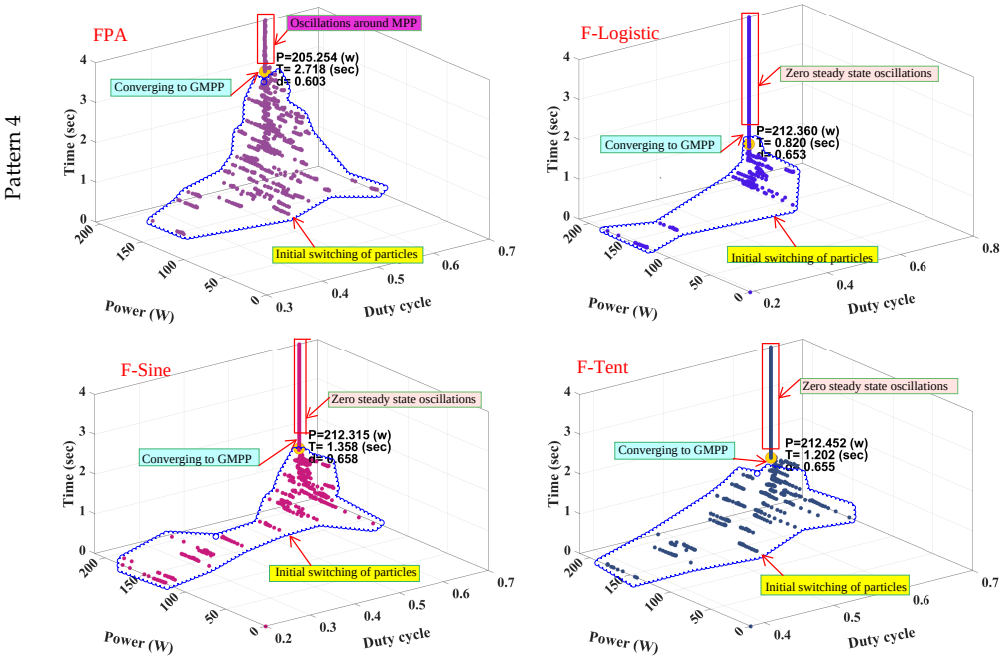

Table 5. *Cont.*

Simulation Analysis for 4S2P Connected SM55 PV Modules	
PSC.	
Pattern 5	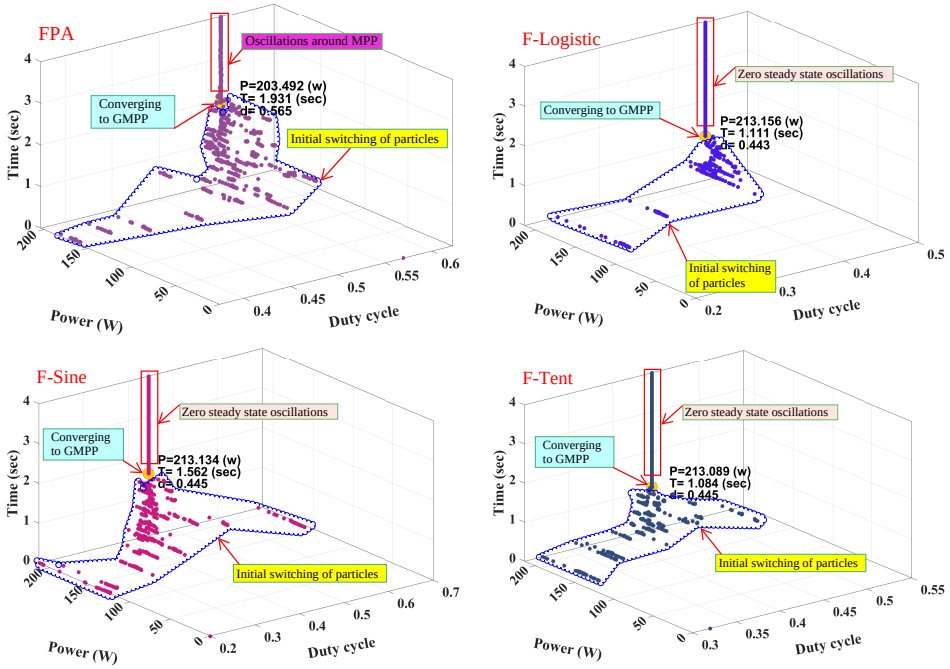

From the presented discussions it can be observed that, the FC-FPA variants exhibits extensive features like, they are not characterized by high initial oscillations and also confirms the tracking maximum power in a shorter period of time irrespective of shade conditions. The oscillations and switching of particles before converging shows high impact on switching devices. The wide range of switching oscillations generates thermal stress over switching devices. which results, failure of switching devices in regular intervals. Introducing the properties of chaotic variants to FPA, it reduces the oscillations of initial switching of particles. Thereby, it reduces thermal stress over the switch, which results improving the life time of switching devices. In addition, FC-FPA variants, shows high stability in searching for the global duty cycle. From the considered 5 patterns, it confirms that, fractional logistic and fractional tent maps show superior performance than other methods. Consequently, utilizing the FC-FPA variants based on the tracker system helps in saving wasted power and cost.

4.1.2. Statistical Analysis

The statistical analysis is the one, which indicates the performance of any system qualitatively. Therefore, authors considered it as important factor to evaluate the performance proposed variants compare with FPA. By performing the calculations using Equations (13)–(16), the obtained values are presented in Table 6 for the 5 shade patterns. The discussion on statistical analysis carried-out using 4S and 4S2P configurations are presented below:

1. **For the 1st configuration 4S connected S36 modules**

   - For Pattern 1, from the presented values in Table 6, it can be noticed that, FC-FPA variants provide the lower values of RMSE and MAE with more reliability compare to FPA. Among the FC-FPA variants, the fractional tent map attains the best STD value 4.547×10^{-10}, high efficiency 99.8976% and consumes less computational time 0.992 s than other methods. Therefore, it confirms the superior performance of FC-FPA tent map.
   - For pattern 2, carrying out the statistical analysis under shade conditions shows the robustness of the proposed variants. From the presented values in Table 6, it confirms that the fractional logistic and fractional tent maps able to achieve lower RMSE, MAE, and STD with higher stability. These maps, takes less computational time than other towards achieving high efficiency.
   - Pattern 3, it is considered as the stronger shade than patterns 1 and 2. Therefore, the obtained results under this pattern ensures the perfectness of proposed variants. From the presented values in Table 6, fractional sine and fractional tent maps almost similar behavior and exhibits excellent performance than FPA. Fractional tent map takes computational time of 1.083 s which very less compare to FPA.

2. **For the 2nd configuration 4S2P connected SM55 modules**

   - Pattern 4, helps to validate the proposed variants qualitatively even under high rated power plants and in case of increasing the complexity of the shade conditions. In pattern 4, FC-FPA variants attain the lower values of RMSE, MAE, and STD. Fractional logistic map attains high efficiency with a computation time of 0.820 s, which is less than other methods. However, fractional tent map shows good stability with higher accuracy as per the results presented in Table 6.
   - For Pattern 5, FC-FPA variants exhibits their efficiency, superiority, and stability in tracking the GMPP under strong shade pattern. The lower values of RMSE, MAE, and STD with an efficiency reaching for 99.8538% confirm the superior performance of FC-FPA with a logistic map.

By the end of this subsection, it confirms that integrating the fractional chaotic maps with the FPA enhances the reliability of the basic technique under all shade conditions. FC-FPA variants exhibits higher power than FPA with shorter tracking time by 50% of that FPA, especially with the fractional logistic and fractional tent maps. Further, introduced variants helps to get rid of higher switching stress over switching devices. Further, the chaotic variants significantly improved system performance and helps to maintain its randomness for any sort of irradiation conditions.

4.2. Validation of Proposed Method under Dynamic Change in Irradiation's

It is a fact that, environmental conditions will not be uniform for long time and it will change often. Therefore, it is mandatory to validate the proposed method, under dynamic change in irradiation's. In order to test the dynamic ability of introduced variants under shade conditions, various simulations have been performed and are discussed as follows:

Table 6. Comparison between MPPT variants over the five patterns.

				Comparable Factors						
String/PSC/Algorithms				$Mean\ P_{pv_{ei}}(w)$	$P_{pv_m}(w)$	$Mean\ \eta(\%)$	$RMSE$	MAE	STD	**Tracking Time (s)**
4S Connected S36 modules	Pattern 1	FPA	FPA	144.908		97.4545	7.05646	3.35738	6.207×10^{0}	3.333
		FC-FPA	F-Logistic	148.513	**148.693**	99.8789	0.18134	0.18134	5.569×10^{-10}	2.342
			F-sine	148.255		99.8256	0.18134	0.18134	5.569×10^{-10}	1.228
			F-tent	**148.514**		**99.8796**	**0.18134**	**0.18134**	$\mathbf{4.547 \times 10^{-10}}$	**0.992**
	Pattern 2	FPA	FPA	69.623		99.8294	0.11853	0.20921	1.724×10^{-1}	2.233
		FC-FPA	F-Logistic	69.710	**69.742**	99.9512	0.03234	0.03234	2.242×10^{-8}	1.413
			F-sine	69.643		99.8580	0.09916	0.16641	1.336×10^{-1}	1.688
			F-tent	**69.710**		**99.9541**	**0.03234**	**0.03234**	$\mathbf{3.562 \times 10^{-8}}$	**1.353**
	Pattern 3	FPA	FPA	56.121		97.40205	3.00158	1.49683	2.602×10^{0}	3.333
		FC-FPA	F-Logistic	57.389	**57.616**	99.60754	0.24425	0.22612	9.234×10^{-2}	1.330
			F-sine	57.465		99.73839	0.15073	0.15073	1.109×10^{-7}	1.681
			F-tent	**57.467**		**99.73839**	**0.15073**	**0.15073**	$\mathbf{1.494 \times 10^{-7}}$	**1.083**
4S2P Connected SM55 modules	Pattern 4	FPA	FPA	205.254		96.4911	16.02929	7.46113	14.18695	2.718
		FC-FPA	F-Logistic	212.360	**212.718**	99.8317	0.36765	0.36765	9.3334×10^{-7}	0.820
			F-sine	212.315		99.8105	0.40161	0.40161	4.16×10^{-2}	1.358
			F-tent	**212.452**		**99.8750**	**0.36765**	**0.36765**	$\mathbf{1.1792 \times 10^{6}}$	**1.202**
	Pattern 5	FPA	FPA	203.492		95.3267	9.96917	12.66596	7.81295	1.931
		FC-FPA	**F-Logistic**	**213.156**	**213.468**	**99.8538**	**0.40030**	**0.40030**	$\mathbf{3.3647 \times 10^{-7}}$	**1.111**
			F-sine	213.134		99.8435	0.40030	0.40030	1.6224×10^{-7}	1.562
			F-tent	**213.089**		**99.8225**	**0.40030**	**0.40030**	$\mathbf{1.2354 \times 10^{-7}}$	**1.083**

Where the mean values of the obtained power and efficiency can be computed by $\sum_{i=1}^{K}(P_{pv_{ei}})/K(w)$ and $\sum_{i=1}^{K}(\eta)/K(\%)$, respectively over number of runs (K). The bold font for the best results and the global values.

4.2.1. 4S Configuration Designed with S36 Modules

In order to test dynamic ability of the proposed method, simulations have been programmed in such a way that, the irradiation distribution changes from pattern 1 to pattern 2 and finally to pattern 3. First, the distribution on the PV array change from pattern 1 to pattern 2 at 2.7 s, while the second step change in the irradiation level occurred at 5.4 s to pattern 3. The step change in irradiation and power convergence curves including duty cycles changes can be observed from the figures presented in Figure 6.

From the figures, it is seen that the FPA method takes longer time to reach MPP and including with high oscillation around MPP. The same behavior is continued during change in patterns. However, the introduced chaotic variants achieved MPP in shorter period of time more importantly with negligible oscillations. In addition, the features of chaotic variants helps the proposed technique to identify the global MPP in a less time. This confirms the strong exploitation ability of the fractional chaotic variants especially in cases of fractional logistics and fractional tent. Moreover, that validates the suitability of proposed variants for the application of MPPT even under high dynamic change in irradiation conditions.

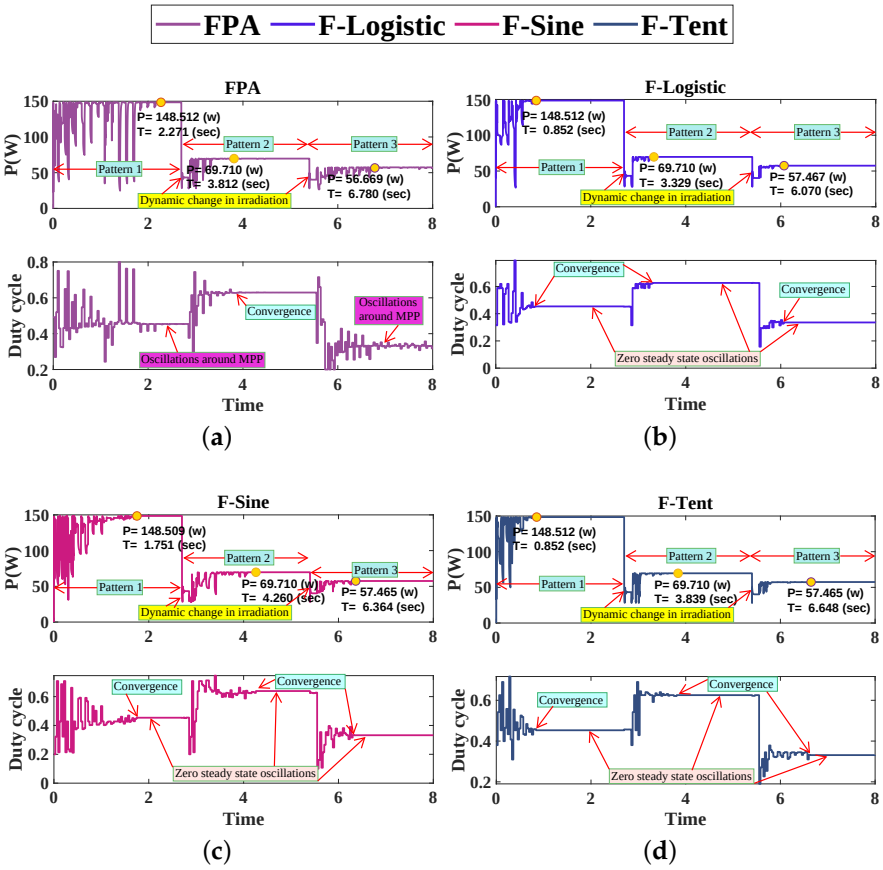

Figure 6. The obtained power and duty cycle by the algorithms over the step changes in irradiance condition from pattern 1 to 2 to 3 in the case of 4S of S36 connected PV array: (**a**) FPA, (**b**) F-logistic map with FPA, (**c**) F-sine map with FPA, and (**d**) F-tent map with FPA.

4.2.2. 4S2P Configuration Design with SM55 Modules

A similar dynamic test is performed with 4S2P configuration to show the robustness, reliability and efficiency of the proposed variants. In this configuration, the system is operated with pattern 4 until 4 s, and then shifted to pattern 5. The obtained convergence curves, which reflects the behavior of proposed method including with FPA is presented in Figure 7. The presented results authenticates the converging the system into a global power. But the, FPA exhibits high amount of oscillations, converges to GMPP for pattern 4 at 2.294 s, after shifted to pattern 5, it failed to reach global and produces continuous oscillations. After occurrence of dynamic change, FPA is able to tack only 178.032 W. FC-FPA variants shows superior performance tracks global power without any oscillations around MPP. After performing dynamic change, FC-FPA variants is able to track 213.286 W, which is much higher than FPA. However, FC-FPA variants, able to track global power for the both pattern 4 and pattern 5. MPPT with fractional chaotic tent map shows faster convergence than other methods then fractional chaotic logistics map. The efficiency of the FC-FPA MPPT methods achieves 99.8% in shorter time meanwhile that of FPA is not exceeded by 98%. With the performed analysis, once again it proves the potential in exploration and exploitation behavior of proposed variants. From the presented results it is noteworthy to mention that, the proposed fractional chaotic variants performs superior performance in terms of GMPP and faster convergence and computational time.

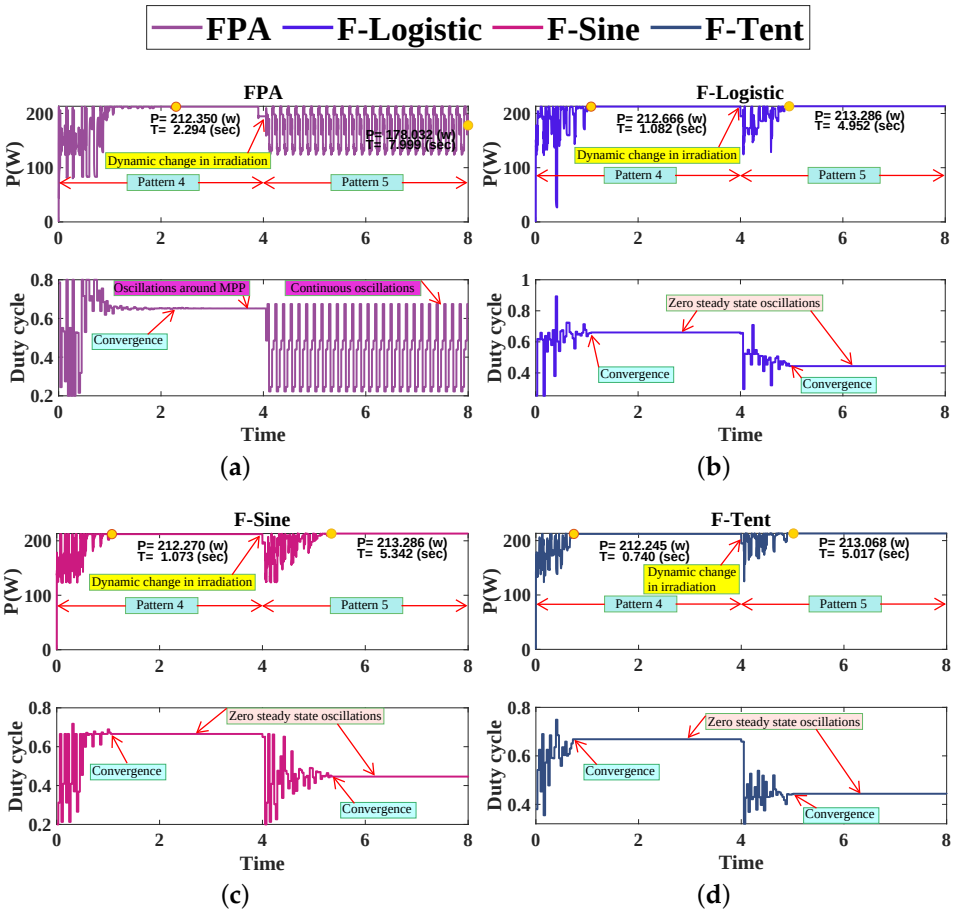

Figure 7. The obtained power and duty cycle by the algorithms over the step changes in irradiance condition from pattern 4 to 5 in the case of 4S2P of SM55 connected PV array: (**a**) FPA, (**b**) F-logistic map with FPA, (**c**) F-sine map with FPA, and (**d**) F-tent map with FPA.

5. Comparison with Traditional Perturb and Observe Technique (P&O)

In this section, the recommended fractional chaotic tent map combined with FPA based MPPT technique compared with the well known traditional Perturb and Observe algorithm (P&O). The considered flowchart of P&O is illustrate at Figure 8.

The comparison is carried out on two aspects, the former one exhibits the results of the algorithm over pattern 5 of 4S2P array reconfiguration. The latter one, however, shows the response of the algorithms during the dynamic change for the irradiance levels from pattern 1 to 2 then to 3 at time samples 2.7 s and 5.4 s from the simulation time as described in Section 4.2.1. The settings of P&O method are the initial duty cycle value (d = 0.5) and the step change in the duty cycle (Δd = 0.0025). The duty cycle selected such that to simplify the task on P&O especially in the dynamical change in the irradinace levels. It is noticed that the global peak exists at duty cycle near to 0.5 from the previous subsections. Therefore, P&O starts the perturbation from this value of duty cycle (d = 0.5).

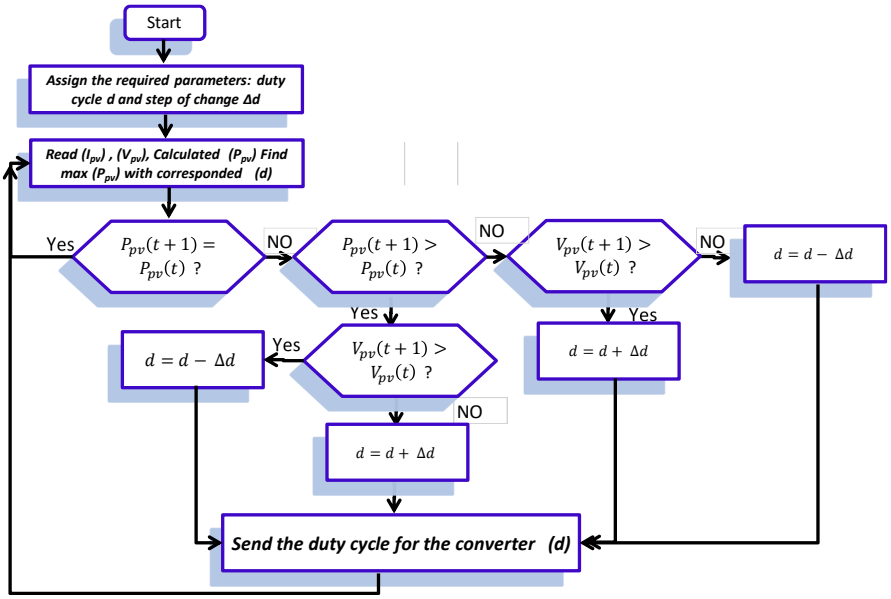

Figure 8. Flowchart of P&O technique.

The response of the implemented P&O and F-tent map over pattern 5 of shading is illustrated in Figure 9. By inspecting the figure it can be seen that, the P&O response reaches the higher value of the power compared to that obtaining by FC-FPA mppt in case of F-tent after longer time of fluctuation.

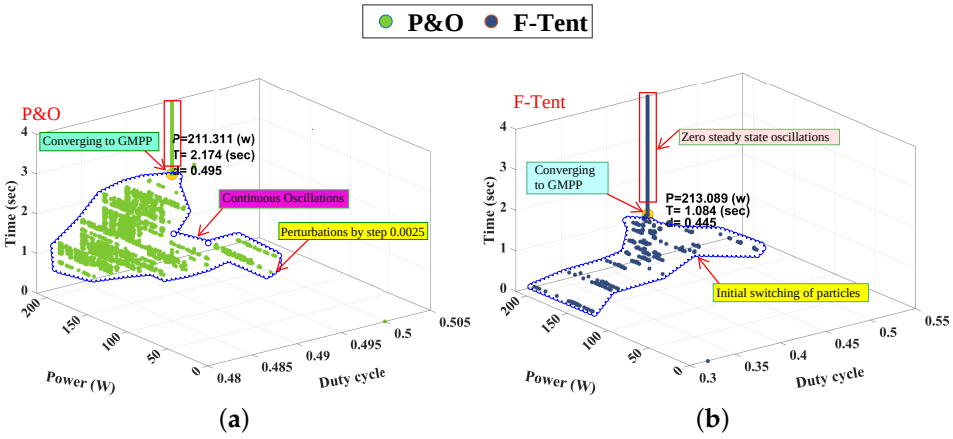

Figure 9. The obtained power and duty cycle by the P&O and the fractional tent map for pattern 5 in the case of 4S2P of SM55 PV array reconfiguration: (**a**) P&O, and (**b**) F-tent map with FPA.

For the dynamical changes in the irradiance levels from patterns 1 to 2 and finally to 3, the dynamical performances by the two considered techniques are shown in Figure 10. The figure indicates the efficiency of the proposed mppt technique with F-tent in tracking the rapid changes in the irradiation levels over the considered modules of the PV array. P&O shows high fluctuation and trapping in local peak. Accordingly, the authors endorse the FC-FPA mppt in case of using the F-tent to overcome the limitations and drawbacks of P&O with rapid change in the shading situations.

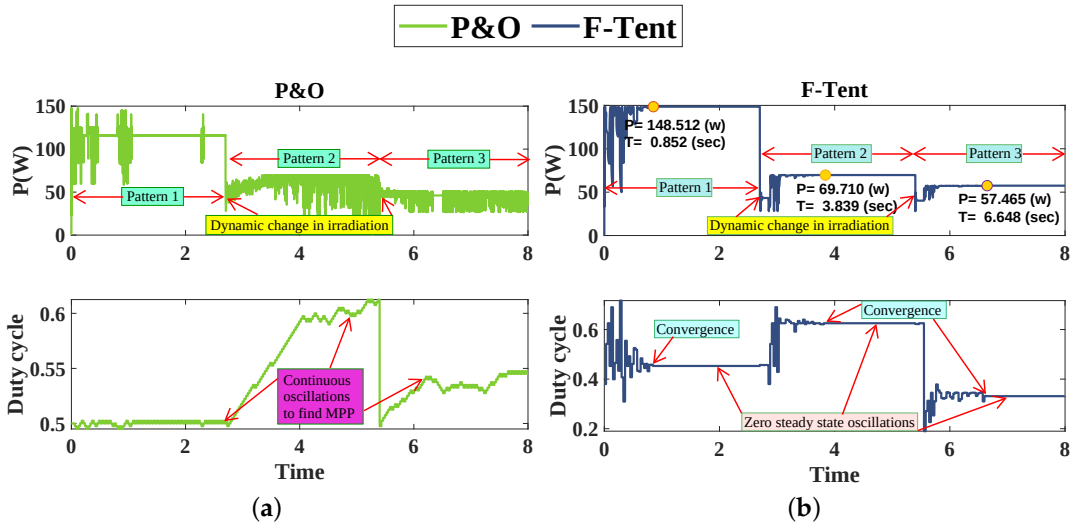

Figure 10. The obtained power and duty cycle by the P&O and the fractional tent map over the step changes in irradiance condition from pattern 1 to 2 to 3 in the case of 4S connected S36 PV array reconfiguration: (**a**) P&O, and (**b**) F-tent map with FPA.

6. Conclusions

In this article, the authors proposed a new algorithm titled "Fractional chaotic Flower Pollination Algorithm" for the first time for the application of maximum power point tracking. Three fractional chaotic (Logistic, Sine, Tent) have been merged with the basic version of FPA to enhance the superiority of FPA. The various simulation studies have been performed by considering two different types (Multi-crystalline and Mono-crystalline) of PV modules made with Shell S36 and Shell SM55. The performance of the proposed system is verified with five different shade patterns with two different configurations of the PV system. Furthermore, assessing the excellence of the proposed method, the qualitative study (Efficiency, RMSE, MAE, STD) have been carried out and compared with basic FPA in all stages of analysis. The dynamic change in irradiation is performed with a combination of three shade pattern. From the obtained results, it confirms that fractional chaotic logistics and fractional tent maps attain high efficiency (99.87%), in tacking GMPP with less computational time near to (1 s) than the FPA for all shade patterns. Further, the FC-FPA recommendsed variants show more consistency, zero oscillations around MPP and avoids LMPP not only over FPA but also over the conventional perturb and observe technique (P&O). Thereby, it can be concluded that merging the fractional chaotic logistic and fractional tent maps with FPA give the best solution to track MPP for any sort of irradiation changes.

Author Contributions: All authors were responsible for conceptualizing the framework, writing and editing, and reviewing the paper.

Funding: This research received no external funding.

Conflicts of Interest: The authors declare there are no conflict of interest

References

1. Ram, J.P.; Babu, T.S.; Rajasekar, N. A comprehensive review on solar PV maximum power point tracking techniques. *Renew. Sustain. Energy Rev.* **2017**, *67*, 826–847. [CrossRef]
2. Islam, H.; Mekhilef, S.; Shah, N.; Soon, T.; Seyedmahmousian, M.; Horan, B.; Stojcevski, A. Performance evaluation of maximum power point tracking approaches and photovoltaic systems. *Energies* **2018**, *11*, 365. [CrossRef]
3. WEO . *World Energy Outlook*; International Energy Agency (IEA): Paris, France, 2018.

4. Selvakumar, S.; Madhusmita, M.; Koodalsamy, C.; Simon, S.P.; Sood, Y.R. High-Speed Maximum Power Point Tracking Module for PV Systems. *IEEE Trans. Ind. Electron.* **2019**, *66*, 1119–1129. [CrossRef]
5. Liu, L.; Meng, X.; Liu, C. A review of maximum power point tracking methods of PV power system at uniform and partial shading. *Renew. Sustain. Energy Rev.* **2016**, *53*, 1500–1507. [CrossRef]
6. Belhachat, F.; Larbes, C. Comprehensive review on global maximum power point tracking techniques for PV systems subjected to partial shading conditions. *Sol. Energy* **2019**, *183*, 476–500. [CrossRef]
7. Guo, L.; Meng, Z.; Sun, Y.; Wang, L. A modified cat swarm optimization based maximum power point tracking method for photovoltaic system under partially shaded condition. *Energy* **2018**, *144*, 501–514. [CrossRef]
8. Alik, R.; Jusoh, A. Modified Perturb and Observe (P&O) with checking algorithm under various solar irradiation. *Sol. Energy* **2017**, *148*, 128–139.
9. Xiao, X.; Huang, X.; Kang, Q. A hill-climbing-method-based maximum-power-point-tracking strategy for direct-drive wave energy converters. *IEEE Trans. Ind. Electron.* **2016**, *63*, 257–267. [CrossRef]
10. Tey, K.S.; Mekhilef, S. Modified incremental conductance MPPT algorithm to mitigate inaccurate responses under fast-changing solar irradiation level. *Sol. Energy* **2014**, *101*, 333–342. [CrossRef]
11. Mohamed, M.A.; Diab, A.A.Z.; Rezk, H. Partial shading mitigation of PV systems via different meta-heuristic techniques. *Renew. Energy* **2019**, *130*, 1159–1175. [CrossRef]
12. Aouchiche, N.; Aitcheikh, M.; Becherif, M.; Ebrahim, M. AI-based global MPPT for partial shaded grid connected PV plant via MFO approach. *Sol. Energy* **2018**, *171*, 593–603. [CrossRef]
13. Priyadarshi, N.; Ramachandaramurthy, V.; Padmanaban, S.; Azam, F. An ant colony optimized MPPT for standalone hybrid PV-wind power system with single Cuk converter. *Energies* **2019**, *12*, 167. [CrossRef]
14. Seyedmahmoudian, M.; Kok Soon, T.; Jamei, E.; Thirunavukkarasu, G.S.; Horan, B.; Mekhilef, S.; Stojcevski, A. Maximum Power Point Tracking for Photovoltaic Systems under Partial Shading Conditions Using Bat Algorithm. *Sustainability* **2018**, *10*, 1347. [CrossRef]
15. Ram, J.P.; Rajasekar, N. A novel flower pollination based global maximum power point method for solar maximum power point tracking. *IEEE Trans. Power Electron.* **2017**, *32*, 8486–8499.
16. Diab, A.A.Z.; Rezk, H. Global MPPT based on flower pollination and differential evolution algorithms to mitigate partial shading in building integrated PV system. *Sol. Energy* **2017**, *157*, 171–186. [CrossRef]
17. Armghan, H.; Ahmad, I.; Armghan, A.; Khan, S.; Arsalan, M. Backstepping based non-linear control for maximum power point tracking in photovoltaic system. *Sol. Energy* **2018**, *159*, 134–141.
18. Fathy, A.; Rezk, H. A novel methodology for simulating maximum power point trackers using mine blast optimization and teaching learning based optimization algorithms for partially shaded photovoltaic system. *J. Renew. Sustain. Energy* **2016**, *8*, 023503. [CrossRef]
19. Chao, K.H.; Wu, M.C. Global maximum power point tracking (MPPT) of a photovoltaic module array constructed through improved teaching-learning-based optimization. *Energies* **2016**, *9*, 986. [CrossRef]
20. Gayathri, R.; Ezhilarasi, G. Golden section search based maximum power point tracking strategy for a dual output DC-DC converter. *Ain Shams Eng. J.* **2017**, *9*, 2617–2630. [CrossRef]
21. Winston, D.P.; Kumar, B.P.; Christabel, S.C.; Chamkha, A.J.; Sathyamurthy, R. Maximum power extraction in solar renewable power system-a bypass diode scanning approach. *Comput. Electr. Eng.* **2018**, *70*, 122–136. [CrossRef]
22. Abdalla, O.; Rezk, H.; Ahmed, E.M. Wind driven optimization algorithm based global MPPT for PV system under non-uniform solar irradiance. *Sol. Energy* **2019**, *180*, 429–444. [CrossRef]
23. Sudhakar Babu, T.; Sangeetha, K.; Rajasekar, N. Voltage band based improved particle swarm optimization technique for maximum power point tracking in solar photovoltaic system. *J. Renew. Sustain. Energy* **2016**, *8*, 013106. [CrossRef]
24. Babu, T.S.; Rajasekar, N.; Sangeetha, K. Modified particle swarm optimization technique based maximum power point tracking for uniform and under partial shading condition. *Appl. Soft Comput.* **2015**, *34*, 613–624. [CrossRef]
25. Ram, J.P.; Rajasekar, N. A new robust, mutated and fast tracking LPSO method for solar PV maximum power point tracking under partial shaded conditions. *Appl. Energy* **2017**, *201*, 45–59.
26. Peng, B.R.; Ho, K.C.; Liu, Y.H. A novel and fast MPPT method suitable for both fast changing and partially shaded conditions. *IEEE Trans. Ind. Electron.* **2018**, *65*, 3240–3251. [CrossRef]

27. Sangeetha, K.; Babu, T.S.; Sudhakar, N.; Rajasekar, N. Modeling, analysis and design of efficient maximum power extraction method for solar PV system. *Sustain. Energy Technol. Assess.* **2016**, *15*, 60–70. [CrossRef]
28. Chaieb, H.; Sakly, A. A novel MPPT method for photovoltaic application under partial shaded conditions. *Sol. Energy* **2018**, *159*, 291–299. [CrossRef]
29. Huang, C.; Wang, L.; Long, H.; Luo, X.; Wang, J.H. A hybrid global maximum power point tracking method for photovoltaic arrays under partial shading conditions. *Optik* **2019**, *180*, 665–674. [CrossRef]
30. Mao, M.; Zhang, L.; Duan, P.; Duan, Q.; Yang, M. Grid-connected modular PV-Converter system with shuffled frog leaping algorithm based DMPPT controller. *Energy* **2018**, *143*, 181–190. [CrossRef]
31. Bahrami, M.; Gavagsaz-Ghoachani, R.; Zandi, M.; Phattanasak, M.; Maranzanaa, G.; Nahid-Mobarakeh, B.; Pierfederici, S.; Meibody-Tabar, F. Hybrid maximum power point tracking algorithm with improved dynamic performance. *Renew. Energy* **2019**, *130*, 982–991. [CrossRef]
32. Martin, A.D.; Vazquez, J.R.; Cano, J. MPPT in PV systems under partial shading conditions using artificial vision. *Electr. Power Syst. Res.* **2018**, *162*, 89–98. [CrossRef]
33. Al-Dhaifallah, M.; Nassef, A.M.; Rezk, H.; Nisar, K.S. Optimal parameter design of fractional order control based INC-MPPT for PV system. *Sol. Energy* **2018**, *159*, 650–664. [CrossRef]
34. Eltamaly, A.M.; Farh, H.M. Dynamic global maximum power point tracking of the PV systems under variant partial shading using hybrid GWO-FLC. *Sol. Energy* **2019**, *177*, 306–316. [CrossRef]
35. Mirjalili, S.; Gandomi, A.H. Chaotic gravitational constants for the gravitational search algorithm. *Appl. Soft Comput.* **2017**, *53*, 407–419. [CrossRef]
36. Yousri, D.; Allam, D.; Eteiba, M.; Suganthan, P.N. Static and dynamic photovoltaic models' parameters identification using Chaotic Heterogeneous Comprehensive Learning Particle Swarm Optimizer variants. *Energy Convers. Manag.* **2019**, *182*, 546–563. [CrossRef]
37. Li, X.; Wen, H.; Hu, Y.; Jiang, L. A novel beta parameter based fuzzy-logic controller for photovoltaic MPPT application. *Renew. Energy* **2019**, *130*, 416–427. [CrossRef]
38. Li, X.; Wen, H.; Hu, Y.; Jiang, L. Drift-free current sensorless MPPT algorithm in photovoltaic systems. *Sol. Energy* **2019**, *177*, 118–126. [CrossRef]
39. Tey, K.S.; Mekhilef, S.; Seyedmahmoudian, M.; Horan, B.; Oo, A.T.; Stojcevski, A. Improved differential evolution-based MPPT algorithm using SEPIC for PV systems under partial shading conditions and load variation. *IEEE Trans. Ind. Inform.* **2018**, *14*, 4322–4333. [CrossRef]
40. Hadji, S.; Gaubert, J.P.; Krim, F. Real-time genetic algorithms-based mppt: Study and comparison (theoretical an experimental) with conventional methods. *Energies* **2018**, *11*, 459. [CrossRef]
41. Alam, D.; Yousri, D.; Eteiba, M. Flower pollination algorithm based solar PV parameter estimation. *Energy Convers. Manag.* **2015**, *101*, 410–422. [CrossRef]
42. Babu, T.S.; Ram, J.P.; Sangeetha, K.; Laudani, A.; Rajasekar, N. Parameter extraction of two diode solar PV model using fireworks algorithm. *Sol. Energy* **2016**, *140*, 265–276. [CrossRef]
43. Allam, D.; Yousri, D.; Eteiba, M. Parameters extraction of the three diode model for the multi-crystalline solar cell/module using Moth-Flame Optimization Algorithm. *Energy Convers. Manag.* **2016**, *123*, 535–548. [CrossRef]
44. De Soto, W.; Klein, S.; Beckman, W. Improvement and validation of a model for photovoltaic array performance. *Sol. Energy* **2006**, *80*, 78–88. [CrossRef]
45. Deshkar, S.N.; Dhale, S.B.; Mukherjee, J.S.; Babu, T.S.; Rajasekar, N. Solar PV array reconfiguration under partial shading conditions for maximum power extraction using genetic algorithm. *Renew. Sustain. Energy Rev.* **2015**, *43*, 102–110. [CrossRef]
46. Babu, T.S.; Ram, J.P.; Dragičević, T.; Miyatake, M.; Blaabjerg, F.; Rajasekar, N. Particle swarm optimization based solar PV array reconfiguration of the maximum power extraction under partial shading conditions. *IEEE Trans. Sustain. Energy* **2018**, *9*, 74–85. [CrossRef]
47. Norouzzadeh, E.; Ahmad, A.A.; Saeedian, M.; Eini, G.; Pouresmaeil, E. Design and Implementation of a New Algorithm for Enhancing MPPT Performance in Solar Cells. *Energies* **2019**, *12*, 519. [CrossRef]
48. Seyedmahmoudian, M.; Rahmani, R.; Mekhilef, S.; Oo, A.M.T.; Stojcevski, A.; Soon, T.K.; Ghandhari, A.S. Simulation and hardware implementation of new maximum power point tracking technique for partially shaded PV system using hybrid DEPSO method. *IEEE Trans. Sustain. Energy* **2015**, *6*, 850–862. [CrossRef]
49. Yang, X.S. Flower pollination algorithm for global optimization. In *Unconventional Computation and Natural Computation*; Springer: Berlin/Heidelberg, Germany, 2012; pp. 240–249.

50. Pourmousa, N.; Ebrahimi, S.M.; Malekzadeh, M.; Alizadeh, M. Parameter estimation of photovoltaic cells using improved Lozi map based chaotic optimization Algorithm. *Sol. Energy* **2019**, *180*, 180–191. [CrossRef]
51. Auslander, J.; Yorke, J.A. Interval maps, factors of maps, and chaos. *Tohoku Math. J. Second Ser.* **1980**, *32*, 177–188. [CrossRef]
52. Yousri, D.; Allam, D.; Eteiba, M. Parameters Identification of Fractional Order Permanent Magnet Synchronous Motor Models Using Chaotic Meta-Heuristic Algorithms. In *Mathematical Techniques of Fractional Order Systems*; Elsevier: Amsterdam, The Netherlands, 2018; pp. 529–558.
53. Yousri, D.; Allam, D.; Eteiba, M. Chaotic whale optimizer variants for parameters estimation of the chaotic behavior in Permanent Magnet Synchronous Motor. *Appl. Soft Comput.* **2019**, *74*, 479–503. [CrossRef]
54. Yousri, D.; AbdelAty, A.M.; Said, L.A.; Elwakil, A.; Maundy, B.; Radwan, A.G. Chaotic Flower Pollination and Grey Wolf Algorithms for parameter extraction of bio-impedance models. *Appl. Soft Comput.* **2019**, *75*, 750–774. [CrossRef]